THE EXTRACELLULAR POTENTIAL FIELD OF THE SINGLE ACTIVE NERVE FIBER IN A VOLUME CONDUCTOR

JOHN CLARK *and* ROBERT PLONSEY

From the Bioengineering Group, Systems Research Center, Case Western Reserve University, Cleveland, Ohio 44106

ABSTRACT The potential field of an active fiber in a uniform medium of infinite extent and within a nerve trunk is calculated from transmembrane potential data. The resulting distributions are given quantitatively. A comparison of both magnitude and field pattern in the nerve trunk and infinite medium environments is made and the effect of interstitial conductivity and nerve trunk diameter on potential magnitudes is considered.

I. THE SINGLE ACTIVE FIBER IN AN EXTENSIVE VOLUME CONDUCTOR

Introduction

A quantitative description of the extracellular field of a single unmyelinated nerve fiber in an extensive volume conductor or in a confined nerve trunk is of interest in electrophysiology. The results of such a study are directly applicable to questions concerning the interaction of active and passive fibers in a nerve trunk and to the interpretation of extracellular potential fields in terms of their sources. This paper is concerned with computations of such fields for the infinite medium and nerve trunk geometries and the dependence of the resultant field on conductivity and geometry parameters.

Mathematical expressions for the desired fields have been derived based on a specification of the in situ values of the inner and outer membrane surface potentials (Clark and Plonsey, 1966). Geselowitz (1966) showed how these equations could be modified so that only the transmembrane potential distribution need be known. This represents a significant improvement since available data appears characteristically, in the form of the transmembrane potential distribution ($\Phi_m(z)$), defined as (Clark and Plonsey):

$$\Phi_m(z) = \Phi_s^i(z) - \Phi_s^o(z) \tag{1}$$

where Φ_e^i and Φ_e^o are the inner and outer membrane surface potentials. The modified potential expressions obtained by Geselowitz are utilized as the basis for computation of the extracellular field set up by an isolated nerve fiber both in an infinite conducting medium and in a confined nerve trunk.

MATHEMATICAL DESCRIPTION OF THE ISOLATED FIBER PROBLEM

In this problem we consider an idealized, infinite circular cylindrical axon of radius a, situated in an essentially infinite volume conductor of specific conductivity σ, and having a specific axoplasmic conductivity σ_i. We assume that the transmembrane potential can be characterized as a propagated action potential and that its waveshape and conduction velocity are known. The extracellular potential field is given as (Geselowitz):

$$\Phi^o(\rho, z) = \frac{1}{2\pi} \int_{-\infty}^{\infty} \frac{F_m(k) K_0(|k|\rho)}{\alpha(|k|a) K_0(|k|a)} e^{-jkz}\, dk \tag{2}$$

where $F_m(k)$ is the Fourier transform of the transmembrane potential distribution (Φ_m) and $\alpha(|k|a)$ is defined as:

$$\alpha(|k|a) \equiv -\left[\frac{\sigma}{\sigma_i} \frac{K_1(|k|a) I_0(|k|a)}{K_0(|k|a) I_1(|k|a)} + 1\right] \tag{3}$$

where K_0 and K_1 are modified Bessel functions of the second kind, orders 0 and 1 respectively, and I_0 and I_1 are modified Bessel functions of the first kind, orders 0 and 1, respectively.[1]

The transmembrane potential distribution is approximated mathematically as the sum of three Gaussian distributions as described in Clark and Plonsey (1966, p. 103). That is,

$$\Phi_m(z) = \sum_{i=1}^{3} A_i e^{-B_i^2 (z-c_i)^2}. \tag{4}$$

The Fourier transform ($F_m(k)$) of this potential distribution is defined as:

$$F_m(k) \equiv \int_{-\infty}^{\infty} \Phi_m(z) e^{+jkz}\, dz \tag{5}$$

---

[1] The definition of $\alpha(|k|a)$ corrects an error in sign which appears in Geselowitz (1966). The error arises in the equation for transmembrane current per unit length (i_m) and is corrected by noting that:

$$\left.\frac{\partial I_0(|k|\rho)}{\partial \rho}\right|_{\rho=a} = |k| I_1(|k|a)$$

$$\text{while} \quad \left.\frac{\partial K_0(|k|\rho)}{\partial \rho}\right|_{\rho=a} = -|k| K_1(|k|a).$$

and upon substitution of equation 4 into 5, it is easily evaluated giving:

$$F_m(k) = \sqrt{\pi} \sum_{i=1}^{3} \frac{A_i}{B_i} e^{-k^2/4B_i^2} e^{jkc_i}. \tag{6}$$

Upon substitution of equation 6 into 2 one obtains:

$$\Phi^o(\rho, z) = \frac{1}{2}\sqrt{\pi} \int_{\infty}^{\infty} \sum_{i=1}^{3} \left[A_i/B_i \frac{K_0(|k|\rho)}{\alpha(|k|a)K_0(|k|a)} e^{-k^2/4B_i^2} \right] e^{-jk(z-c_i)}\, dk. \tag{7}$$

Noting that the portion of the integrand in brackets in equation 7 is an even function of k and letting $y = ka$, this equation may be rewritten as:

$$\Phi^o(\rho, z) = 1/\sqrt{\pi}a \int_0^{\infty} \sum_{i=1}^{3} \left[\frac{A_i}{B_i} \frac{K_0\left(\frac{y\rho}{a}\right)}{\alpha(y)K_0(y)} e^{-y^2/4a^2B_i^2} \right] \cos \frac{y(z - c_i)}{a}\, dy \tag{8}$$

where

$$\alpha(y) = -\left[\frac{\sigma K_1(y)I_0(y)}{\sigma_i K_0(y)I_1(y)} + 1 \right]. \tag{9}$$

Thus, equation 8 is the derived expression for potential throughout the external medium in which the single active fiber lies.

SYNTHETIC AXON DATA

Since equation 8 is too complex to permit a general solution we proceed by choosing a typical problem for which $\Phi_m(z)$ is available in the literature. The experiments of Watanabe and Grundfest (1961) on the crayfish lateral giant axon provide a suitable example and the necessary data. The specific values chosen for the constants a, σ, and σ_i are:

$a = 60\ \mu$ (radius of lateral giant axon),

$\sigma = 0.05$ mho/cm (specific conductivity of sea water bathing medium),

$\sigma_i = 0.010$ mho/cm (specific conductivity of axoplasm).

The values of the constants A_i, B_i, c_i in equation 4 that result in a close fit to the monophasic action potential obtained from Watanabe and Grundfest were found to be

$A_1 = 51.0$ mv	$B_1 = 8.0$ cm^{-1}	$c_1 = 0.54$ cm
$A_2 = 72.0$ mv	$B_2 = 5.33$ cm^{-1}	$c_2 = 0.66$ cm
$A_3 = 18.0$ mv	$B_3 = 3.33$ cm^{-1}	$c_3 = 0.86$ cm.

A plot of the above Gaussian approximation appears in Fig. 1.

APPROXIMATIONS FOR NUMERICAL ANALYSIS

Before numerical evaluation of the integral in equation 8 can proceed, it is necessary to replace the infinite limits by suitable finite values. We consider the integral in equation 8 as replaced by the sum of two integrals with limits (0, L) and (L, ∞). Now, if the second integral is negligible compared to the first, then L represents an upper bound on the variable y, such that, for all practical purposes, the desired

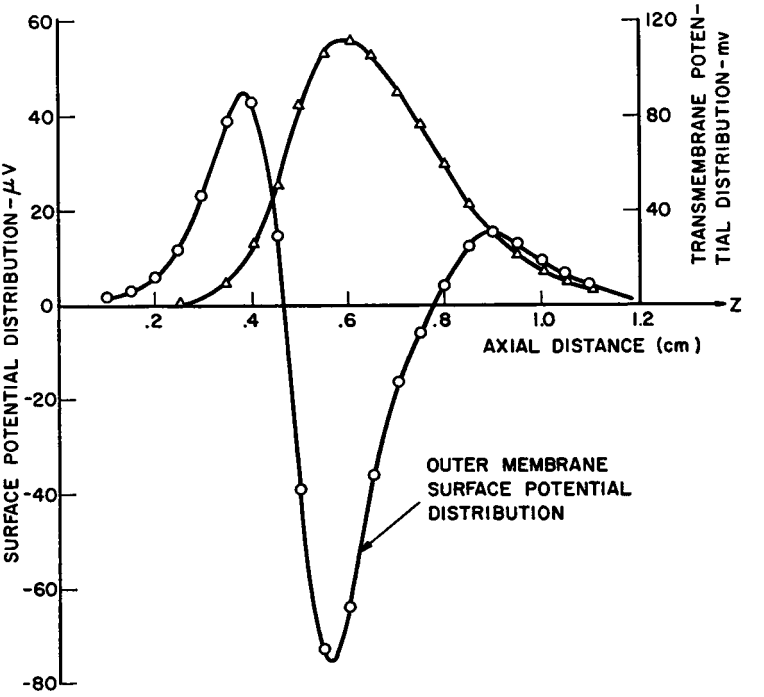

FIGURE 1 Transmembrane and surface potential distributions for the isolated axon example. For the transmembrane potential, △ denotes data points adapted from Watanabe and Grundfest and the solid line represents the Gaussian approximation of equation 4.

solution is given by integrating from zero to L. In the results to be presented the upper bound was determined by numerically evaluating and plotting the integrand of equation 8 as a function of y for various values of ρ and z. For the range of values of ρ and z of interest, $L = 0.3$ was found to be satisfactory. Thus, equation 8 may be approximated by

$$\Phi^{o}(\rho, z) = 1/\sqrt{\pi}a \int_0^{0.3} \sum_{i=1}^{3} \frac{A_i}{B_i} \left[\frac{K_0\left(\frac{y\rho}{a}\right)}{\alpha(y)K_0(y)} e^{-y^2/4a^2B_i^2} \right] \cos y \frac{(z - c_i)}{a} dy \quad (10)$$

where $\alpha(y)$ is given by equation 9.

In the above integration, numerical evaluation of the modified Bessel functions was performed by utilizing one of a number of currently available computer subroutines for this purpose.[2] These are capable of excellent accuracy over the range of argument that enters into equation 10.

[2] These Bessel function subroutines are available in a number of machine languages (Algol 60, Fortran, etc.). The particular procedure used in this study was a modified Fortran subroutine obtained from the Computing Center, Case WRU, Cleveland, Ohio 44106.

RESULTS

Numerical Evaluation of the External Potential Field

The computed outer membrane surface potential distribution obtained from equation 10 utilizing the data noted was found to be triphasic as can be seen from Fig. 1. This resultant form is as expected from experiments reported in the literature.[3] It is of interest to note that this triphasic waveform proceeds directly from the monophasic transmembrane action potential.

The order of magnitude of the extracellular field is seen from Fig. 1 to be under 100 μv and therefore is less than 0.1% of the magnitude of the transmembrane potential. This also agrees qualitatively with data available in the literature.[4] In view of the fact that the potentials are in the low microvolt range one can appreciate the difficulty in mapping such fields experimentally. Indeed a full three-dimensional plot is yet to be attained. The methodology that has been developed here provides for the conversion of the transmembrane potential, which can be determined fairly precisely, into an equally precise extracellular potential distribution, that one has difficulty measuring precisely. Although equation 10 is valid only for an infinite circular cylindrical geometry, this technique should apply generally.

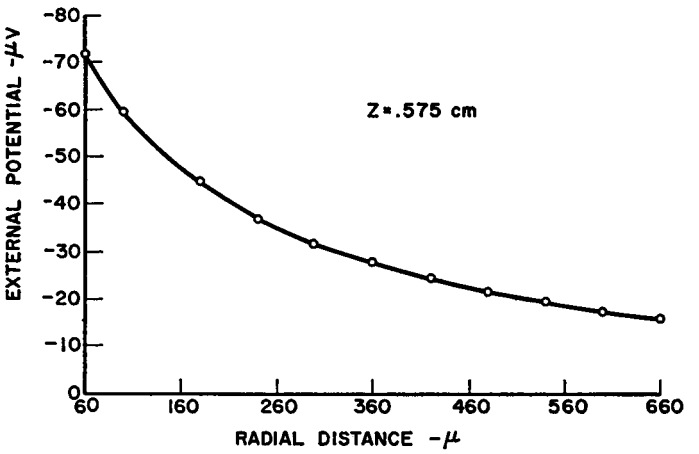

FIGURE 2 Plot of radial fall-off in external potential at $z = 0.575$ cm. (Outer membrane surface of axon is located at $r = 60$ μ.)

While the magnitude of potential determined here is quite low, this is clearly a consequence of the assumed conductivities and the infinite geometry. Changes in conductivity in the physiological range could affect the result by perhaps an order of magnitude. However, even greater changes in the potential magnitude can be produced if the external medium is severely limited, as for the nerve trunk situation. These effects are considered in greater detail in a later section.

[3] See, for example, Tasaki (1959), p. 105. For a simple explanation of the genesis of the triphasic extracellular surface potential, see Brazier (1960) or Offner (1954).

[4] See, for example, Tasaki (1964), Tasaki (1953), Casella and Taccardi (1965).

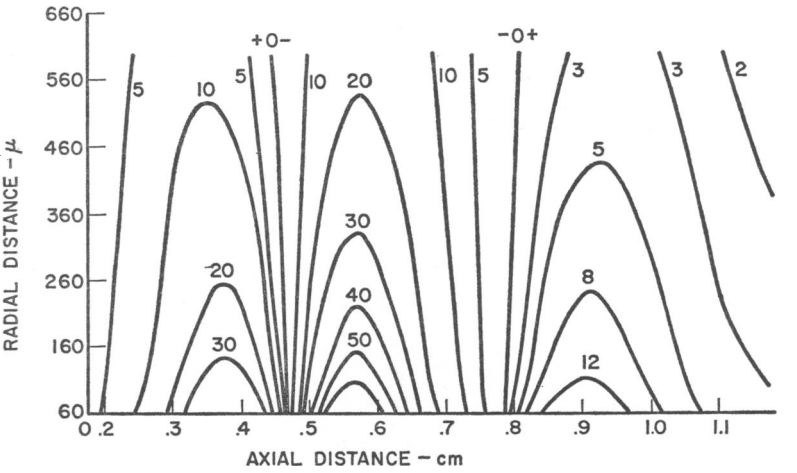

FIGURE 3 Calculated external potential field of 120 μ crayfish lateral giant axon immersed in an extensive volume of sea water for various values of radial distance (r) and axial distance (z). The values of the isopotential lines in this figure are in microvolts. Since the radius of the axon is 60 μ, the radial distance $r = 60\ \mu$ corresponds to the outer membrane surface of the axon.

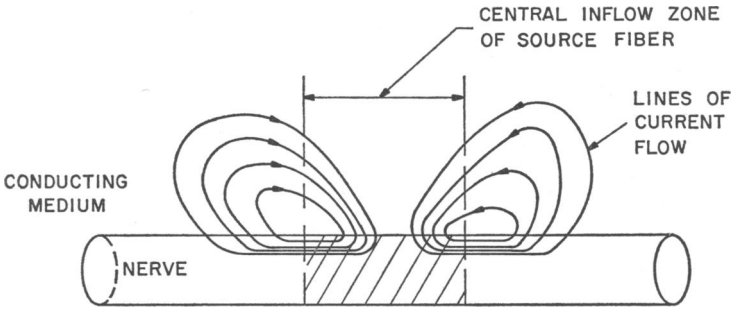

FIGURE 4 Schematic illustration of the current flow lines from an isolated axon in situ (adapted from Offner).

The magnitude of potential was also found to decrease steadily with increasing radial distance from the outer membrane surface ($\rho = 60\ \mu$). From Fig. 2, one can see that the magnitude of the potential evaluated at $z = 0.575$ cm is down to 20% of its value at the membrane surface in roughly 6.25 cell diameters. This general behavior conforms to that found by Lorente de Nó (1947).

The external potential field plot is given in Fig. 3, and appears to be composed of three distinct zones that are delineated by two zero isopotential lines located at $z = 0.46$ and $z = 0.78$ cm. Since the current density field is orthogonal to the potential field it, too, consists of three zones. One can identify a central current inflow flanked by two current outflow zones. Current enters the cell in the central zone (this corresponding to an influx of sodium ions in the active region) and leaves in the zones adjacent to this region. The pattern is consistent with the concept of local circuit current flow[5] (see Fig. 4). This computed potential field plot is in general agreement

[5] A concept used to explain the electrogenesis of propagated action potential.

with the findings of Lorente de Nó (1947) on the frog sciatic nerve trunk. A quantitative comparison between the two cannot be made however since actual magnitudes were not given by Lorente de Nó and because each involve quite different preparations.

Evaluation of Transmembrane Current

The transmembrane current per unit length (i_m) may be evaluated by application of Ohm's law to equation 2 and evaluating at the membrane; the result is:

$$i_m(z) = -2a\left(\sigma \frac{\partial \Phi^o(\rho, z)}{\partial \rho}\bigg|_{\rho=a}\right) \tag{11}$$

$$i_m(z) = \sigma a \int_{\infty}^{\infty} \left[\frac{|k|F_m(k)K_1(|k|a)}{\alpha(|k|a)K_0(|k|a)}\right] e^{-ikz}\, dk \tag{12}$$

where $\alpha(|k|a)$ is given by equation 3 and $F_m(k)$ can be approximated by equation 6. Substituting equation 6 into 12 one obtains

$$i_m(z) = \sqrt{\pi}\sigma a \int_{\infty}^{\infty} \sum_{i=1}^{3} \frac{A_i}{B_i}\left[\frac{|k|K_1(|k|a)}{\alpha(|k|a)K_0(|k|a)} e^{-k^2/4B_i^2}\right] e^{-ik(z-c_i)}\, dk \tag{13}$$

Noting that the portion of the integrand in brackets is an even function of k and letting $y = ka$, this equation may be rewritten for computational purposes as:

$$i_m(z) = \frac{2\sqrt{\pi}\sigma}{a} \int_0^{0.3} \sum_{i=1}^{3} \frac{A_i}{B_i}\left[\frac{yK_1(y)}{\alpha(y)K_0(y)} e^{-y^2/4a^2B_i^2}\right] \cos y(z - c_i)\, dy \tag{14}$$

where $\alpha(y)$ is given by equation 9.

The results of the evaluation of equation 14 for the geometry and parameters given earlier are plotted in Fig. 5. As can be seen, the spatial distribution of i_m is triphasic and furthermore, proportional to the second derivative of the transmembrane potential with respect to z. Core conductor theory predicts that i_m be proportional to the second derivative of transmembrane potential ($\partial^2\Phi_m/\partial z^2$) and the triphasic nature of i_m is an immediate consequence (Tasaki, 1959, p. 104). The specific relationship that can be derived from the cable equations is (Clark and Plonsey, 1966):

$$i_m = \left(\frac{1}{r_i + r_o}\right)\frac{\partial^2 \Phi_m}{\partial z^2} \tag{15}$$

where r_i and r_o are the internal and external longitudinal resistances per unit length (see Fig. 6). Since the axoplasmic current is reasonably uniform and axial we have

$$r_i = \rho_i/A_i \tag{16}$$

where ρ_i is the specific axoplasmic resistivity (ohm·cm) and A_i the internal cross-sectional area (cm²). For the infinite volume conductor situation, r_o should be

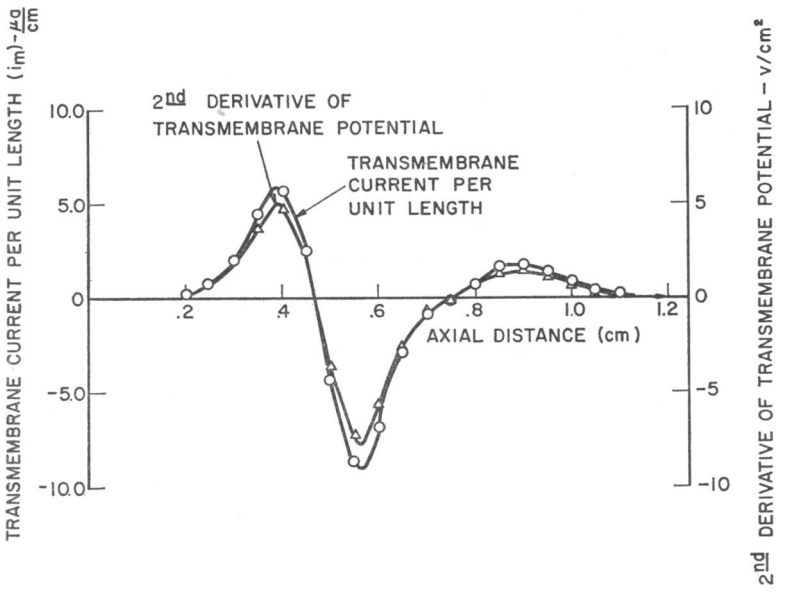

FIGURE 5 The plot of transmembrane current per unit length (i_m) and the second derivative of $\Phi_m(z)$ vs. axial distance z.

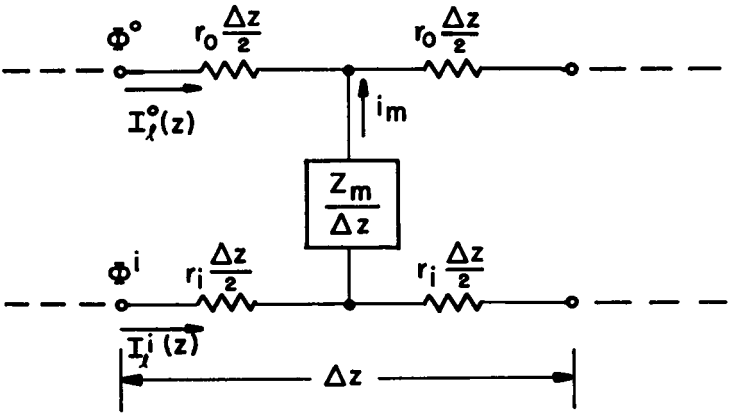

FIGURE 6 The linear core conductor model.

negligible compared to r_i in view of the large effective cross-sectional area of the external medium. For the values used here of $\rho_i = 94$ ohm·cm and $A_i = 0.000113$ cm² (corresponding to a 120 μ diameter axon), r_i evaluates to 8.32×10^5 ohm/cm. This value corresponds quite well with the value of 8.34×10^5 obtained from Fig. 5.[6] This result also confirms that $r_o \ll r_i$ and hence is negligible, a fact that is already clear from the very low values of extracellular potential.

[6] For example, at $z = 0.55$ cm, $i_m = -8.57$ μa/cm and $\partial^2\Phi_m/\partial z^2 = -7.15$ v/cm². Thus from equation 15, we obtain a value of 8.34×10^5 ohm/cm for r_i. This value is found to be fairly uniform with z.

II. THE SINGLE ECCENTRIC FIBER IN A NERVE TRUNK

Introduction

The previous section considered the volume conductor fields of an active fiber in a medium of infinite extent. This section is concerned with the fields produced by a cylindrical fiber eccentrically located within a cylindrical nerve trunk. A sketch of the cross-sectional geometry is shown in Fig. 7.

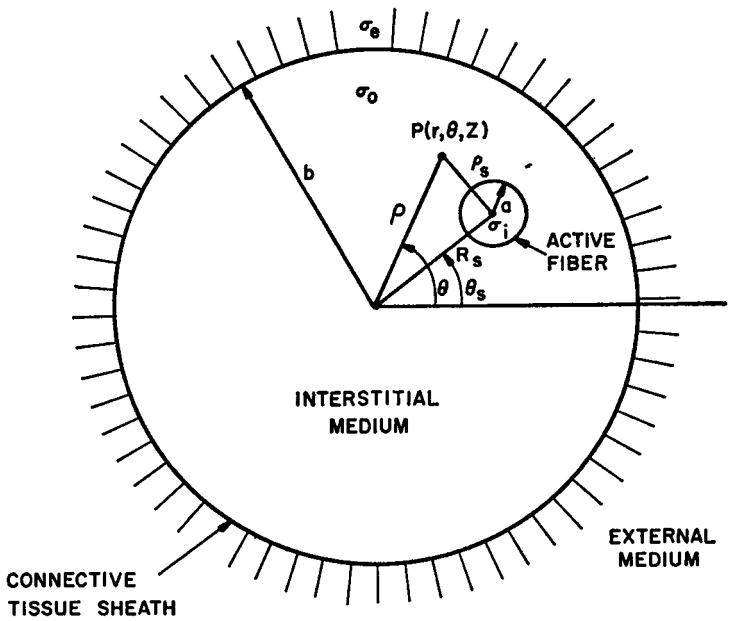

FIGURE 7 Nerve trunk geometry.

The problem to be discussed is of interest since it involves the determination of the field (surrounding the active fiber) in which neighboring fibers lie. It thus forms an important step in the investigation of fiber interaction within a nerve trunk. As we shall see, the magnitude of the field is greatly enhanced, in comparison with the infinite medium, so that a greater potential for interaction effects exists.

MATHEMATICAL FORMULATION

As illustrated in Fig. 7, we consider a single nerve fiber of radius a, situated a distance R_s from the center of a circular cylindrical nerve trunk of radius b. The nerve trunk is assumed to consist of a resistive-capacitive connective tissue sheath at $\rho = b$ (see Fig. 8) and an interstitial bathing fluid medium possessing an average conductivity σ_o. The nerve fiber has an axoplasmic conductivity σ_i. Furthermore, the trunk itself is assumed to be immersed in an extensive uniform conducting medium of conductivity σ_e.

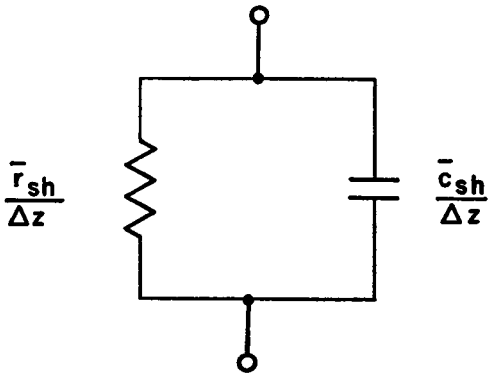

FIGURE 8 The resistive-capacitative nerve trunk sheath. Here $\bar{r}_{sh}$ is the specific resistance (ohm·cm²) and $\bar{C}_{sh}$, the specific capacity ($\mu F/cm^2$) of the sheath.

The radius vector R_s to the center of the active fiber makes an angle θ_s with respect to the horizontal. The field point $P(\rho, \theta, z)$ is located a distance ρ_s from the center of the active source fiber. Employing the law of cosines, the relationship between ρ, R_s and ρ_s is:

$$\rho_s^2 = \rho^2 + R_s^2 - 2\rho R_s \cos(\theta - \theta_s). \tag{17}$$

The general expression for potential in the interstitial medium of the nerve trunk (this region excludes the volume occupied by the "source" fiber), is given as:

$$\Phi^o(\rho, \theta, z) = \Phi_s(\rho, \theta, z) + \sum_{n=0}^{\infty} \cos n(\theta - \theta_s) \int_{-\infty}^{\infty} A_n(k) I_n(|k|\rho) e^{-jkz}\, dk \tag{18}$$

where the $A_n(k)$ are the undetermined potential "coefficients," the $I_n(|k|\rho)$ are the modified Bessel functions of the first kind, order n, and $\Phi_s(\rho, \theta, z)$ is the potential distribution of the source fiber considered as lying in an extensive medium of conductivity σ_o.[7] The second term in equation 18 represents a general solution to Laplace's equation in a bounded cylindrical region. If we replace ρ in equation 2 by the quantity ρ_s (which is appropriate here), then

$$\Phi_s(\rho, \theta, z) = \Phi_s(\rho_s, z) = \frac{1}{2\pi} \int_{-\infty}^{\infty} \frac{F_m(k) K_0(|k|\rho_s)}{\alpha(|k|a) K_0(|k|a)} e^{-jkz}\, dk. \tag{19}$$

Letting $G(k)$ be defined as:

$$G(k) = \frac{F_m(k)}{2\pi\alpha(|k|a) K_0(|k|a)}, \tag{20}$$

[7] Here we tacitly assume that the source generators within the active fiber are independent of the nerve trunk geometry (Lorente de Nó, 1947).

the expression for the source fiber potential becomes:

$$\Phi_s(\rho_s, z) = \int_{-\infty}^{\infty} G(k)K_0(|k|\rho_s)e^{-jkz}\,dk \tag{21}$$

upon substitution of equation 20 into 19.

Since ρ and ρ_s are related by equation 17, the modified Bessel function $K_0(|k|\rho_s)$ may be rewritten as follows (Gray and Matthews, 1966, p. 101):

$$K_0(|k|\rho_s) = \sum_{n=0}^{\infty} (2 - \delta_n{}^0)\cos n(\theta - \theta_s)K_n(|k|R_s)I_n(|k|\rho) \quad \text{for} \quad \rho < R_s \tag{22}$$

$$K_0(|k|\rho_s) = \sum_{n=0}^{\infty} (2 - \delta_n{}^o)\cos n(\theta - \theta_s)I_n(|k|R_s)K_n(|k|\rho) \quad \text{for} \quad \rho > R_s \tag{23}$$

where $\delta_n{}^0 = 1$ for $n = 0$, and $\delta_n{}^o = 0$ for $n \neq 0$.

Upon substitution of equations 22 and 23 into 21 we obtain the following expressions for source fiber potential in terms of ρ, θ, and z. That is,

$$\Phi_s(\rho, \theta, z) = \sum_{n=0}^{\infty} (2 - \delta_n{}^0)\cos n(\theta - \theta_s) \cdot \int_{-\infty}^{\infty} G(k)K_n(|k|R_s)I_n(|k|\rho)e^{-jkz}\,dk \quad \text{for} \quad \rho < R_s \tag{24}$$

$$\Phi_s(\rho, \theta, z) = \sum_{n=0}^{\infty} (2 - \delta_n{}^o)\cos n(\theta - \theta_s) \cdot \int_{-\infty}^{\infty} G(k)I_n(|k|R_s)K_n(|k|\rho)e^{-jkz}\,dk \quad \text{for} \quad \rho > R_s. \tag{25}$$

The general expression for potential in the external medium ($\rho > b$) is:

$$\Phi^e(\rho, \theta, z) = \sum_{n=0}^{\infty} \cos n(\theta - \theta_s) \int_{-\infty}^{\infty} B_n(k)K_n(|k|\rho)e^{-jkz}\,dk \tag{26}$$

where the $B_n(k)$ are the undetermined "coefficients." The functions $A_n(k)$ and $B_n(k)$ remain to be determined to complete the mathematical solution. These functions are evaluated by applying appropriate boundary conditions.

BOUNDARY CONDITIONS

The boundary conditions at $\rho = b$ are: (*a*) Current crossing the connective tissue sheath is assumed to be continuous. That is, since the sheath is very thin, longitudinal currents are assumed to be negligible and therefore all radial current entering the sheath at the interstitial surface must leave the sheath at the outer surface. This condition is expressed mathematically as:

$$-\sigma_o \frac{\partial \Phi^o}{\partial \rho}\bigg|_{\rho=b} = -\sigma_e \frac{\partial \Phi^e}{\partial \rho}\bigg|_{\rho=b} = J_{sh}(\theta, z) \tag{27}$$

where J_{sh} is the trans-sheath current density (amp/cm^2).

(*b*) The sheath is modeled as a distributed, parallel resistance-capacitance network (Fig. 8). Corresponding to a trans-sheath potential defined as:

$$\Phi_{sh}(\theta, z) = \Phi^o(b, \theta, z) - \Phi^e(b, \theta, z), \tag{28}$$

one must then have a trans-sheath current density given by

$$J_{sh}(\theta, z) \equiv \bar{\sigma}_{sh}\, \Phi_{sh}(\theta, z) + \bar{C}_{sh} \frac{\partial \Phi_{sh}(\theta, z)}{\partial t} \tag{29}$$

where $\bar{\sigma}_{sh}$ is the specific conductivity per unit area (mho/cm^2) and $\bar{C}_{sh}$, the capacity per unit area (μF/cm^2) of the sheath.

The time derivative in equation 29 may be evaluated since we assume the existence of a propagated action potential and therefore, all field quantities must vary as $(z + vt)$, where v is the velocity of propagation (in the negative z direction). Thus for a field quantity gr 47 (ρ, θ, z), we have

$$\psi(\rho, \theta, z, t) = \psi[\rho, \theta, (z + vt)] \tag{30}$$

and consequently, as may be readily verified

$$\frac{\partial \psi}{\partial t} = v \frac{\partial \psi}{\partial z}. \tag{31}$$

Thus, equation 29 becomes

$$J_{sh}(\theta, z) = \bar{\sigma}_{sh}\, \Phi_{sh}\, (\theta, z) + v\bar{C}_{sh} \frac{\partial \Phi_{sh}(\theta, z)}{\partial z}. \tag{32}$$

Substituting equation 32 into 27 one obtains the following two equations which we employ as our boundary conditions at $\rho = b$.

$$\sigma_o \frac{\partial \Phi^o}{\partial \rho}\bigg|_{\rho=b} + \bar{\sigma}_{sh}\, \Phi_{sh} + v\bar{C}_{sh} \frac{\partial \Phi_{sh}}{\partial z} = 0 \tag{33}$$

$$\sigma_e \frac{\partial \Phi^e}{\partial \rho}\bigg|_{\rho=b} + \bar{\sigma}_{sh}\, \Phi_{sh} + v\bar{C}_{sh} \frac{\partial \Phi_{sh}}{\partial z} = 0 \tag{34}$$

With the preceeding equations, it is possible to solve for the unknown functions $A_n(k)$ and $B_n(k)$. When substituted into equations 27–29, expressions for interstitial (Φ^o) and external (Φ^e) potential are obtained. These equations are listed in the Appendix. (See equations A1, A2, and A3). The trans-sheath potential can be evaluated via equation 28 and is given in the Appendix by equation A11.

SYNTHETIC DATA FOR THE NERVE TRUNK PROBLEM

As in the isolated axon problem, a realistic nerve trunk example was formulated using data obtained from the literature. The following values were chosen for the geometrical parameters of the model: $a = 60\ \mu$ (radius of source fiber), $b = 300\ \mu$ (radius of nerve trunk), $R_s = 150\ \mu$ (distance from origin to center of active fiber), $\theta_s = 0^o$ (angle R_s makes with horizontal).

Since electric parameters for the crayfish ventral nerve cord are not available in the literature, the following represent educated guesses based, in part, on data for the frog sciatic nerve trunk (Patlak, 1955). We choose $\sigma_i = 0.0106$ mho/cm, $\sigma_o = 0.0250$ mho/cm, $\sigma_e = 0.0500$ mho/cm (sea water bathing medium), $\sigma_{sh} = 0.0010$ mho/cm^2, $\bar{C}_{sh} = 0.02\ \mu$F/cm^2.

For the parameter σ_o, the averaged interstitial conductivity, we assume a value of one-half the conductivity of the sea water bathing medium based on a recognition that the interstitial medium contains interstitial fluid, connective tissue, blood vessels, as well as other inactive fibers. We expect, in general, that $\sigma_e > \sigma_o > \sigma_i$.

NUMERICAL EVALUATION OF THE POTENTIAL EXPRESSIONS

With the assumed data above, the derived expressions for interstitial and external potential (equations A1, A2, and A3) were numerically evaluated in a manner entirely analogous to that of the isolated axon example. The limits of integration used were determined by numerically evaluating and plotting the integrand of these equations as described in the previous section. The values found in this manner were (0, 1.5).

DISCUSSION OF RESULTS

Numerical Evaluation of the Interstitial (Φ^o) and External (Φ^e) Potential Fields

The cross-sectional and longitudinal potential fields in the interstitial medium are shown in Figs. 10 and 11, respectively. In Fig. 9, Φ^o is shown as a function of ρ and θ in the plane $z = 0.625$ cm. From this figure one observes that the presence of the sheath has a pronounced effect on the distribution and magnitude of the field of the source fiber. One notes, for example the significant distortion of the field by the presence of the highly resistive (1000 ohm·cm^2) connective tissue sheath. From the configuration of the field plot one concludes that action currents tend to remain within the trunk. This is reflected in the very small values of external potential Φ^e (in contrast to interstitial potential Φ^o) as computed and tabulated in Table I.

Magnitude of Interstitial Potential

Possibly the most significant feature of Figs. 9 and 10, as well as Table I, is the magnitude of the interstitial potential (Φ^o). Potentials within this medium are found as high as 1500 μv for this particular example. This is in contrast to the maximum extracellular potential values of approximately 70 μv for the isolated fiber. The reason for this large (approximately 20-fold) increase in magnitude is attributed to the increased *effective* resistance of the bathing medium. This conclusion arises from the following considerations.

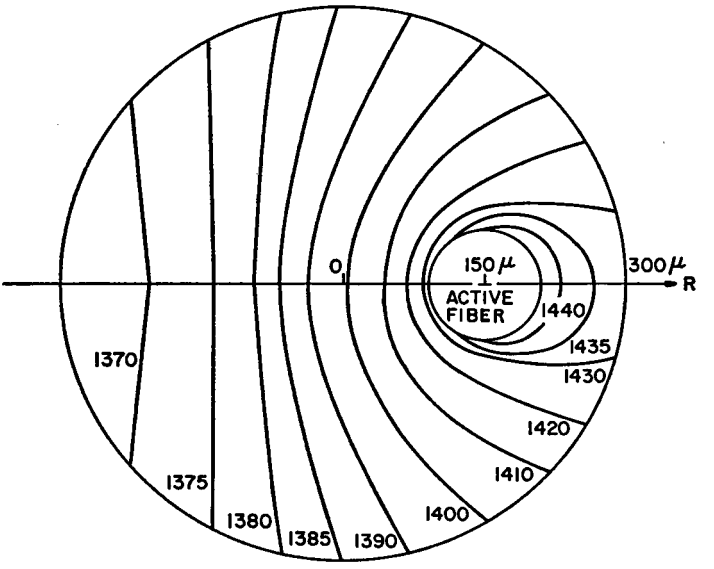

FIGURE 9 Cross-sectional aspect of the potential field within the nerve trunk at $z = 0.625$ cm. The values associated with the isopotential lines in this figure are in microvolts.

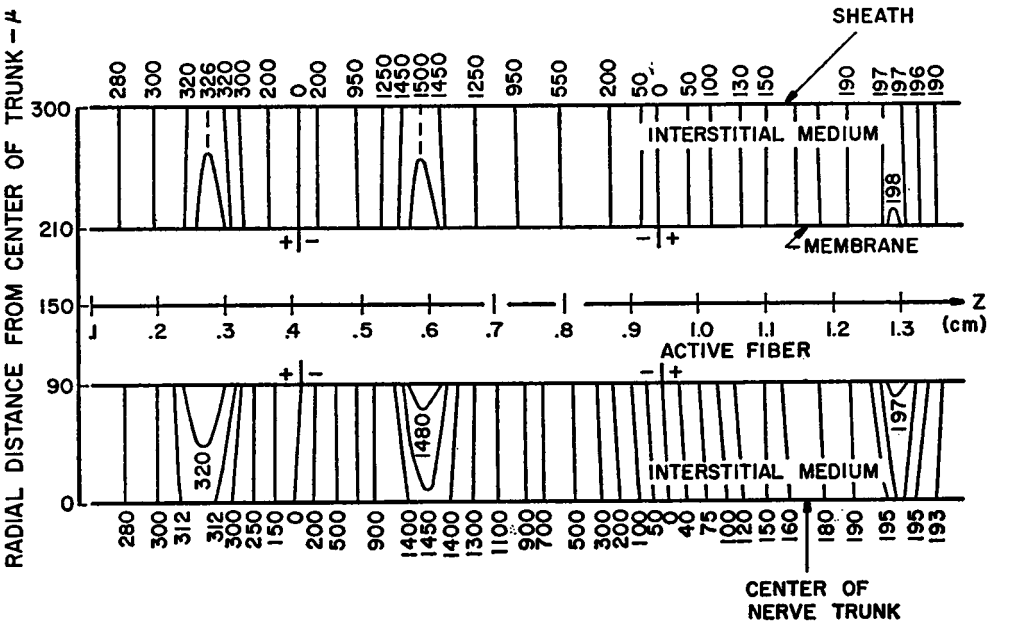

FIGURE 10 Longitudinal aspect of the potential field within the nerve trunk in the plane $\theta = 0°$. The potential field of one-half of the nerve trunk is shown (the half containing the active source fiber). Potential values are in microvolts. One will note that the magnitude of potentials in the region 210–300 μ is slightly larger than that in the region 0–90 μ, due to the concentrating influence of the connective tissue sheath.

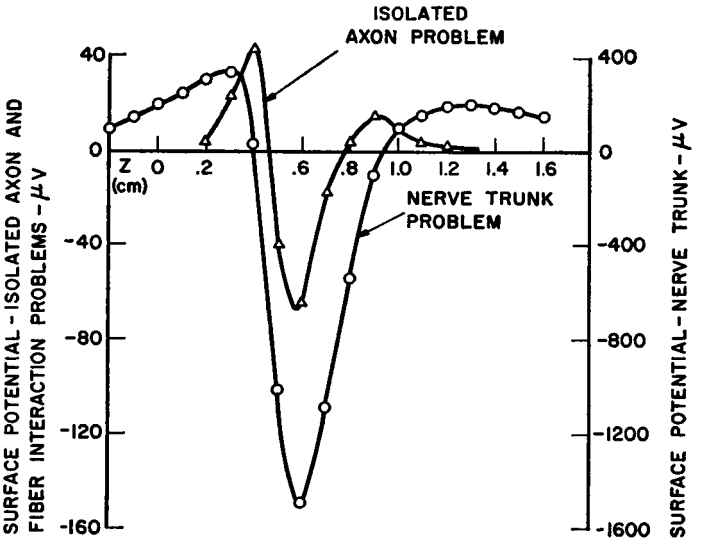

FIGURE 11 A comparison of the outer membrane surface potential distributions for the source fiber in the infinite and nerve trunk environment.

TABLE I

A COMPARISON OF CALCULATED VALUES OF INTERSTITIAL (Φ^o) AND EXTERNAL (Φ^e) POTENTIAL AS A FUNCTION OF ANGLE θ FOR ρ = 300 μ AND z = 0.625 cm

θ	Φ^o	Φ^e
degrees	*microvolts*	*microvolts*
0	1434.1	1.71
30	1421.5	1.71
60	1400.7	1.71
90	1385.4	1.70
120	1374.8	1.69
150	1369.2	1.69
180	1367.1	1.69

Under the assumption that all other factors remain constant, the specific resistivity ($\rho_o = 1/\sigma_o$) and nerve trunk radius (b) were varied about their assumed values so that their effect on the general magnitude of Φ^o could be determined. The results are given in Figs. 12 and 13. In Fig. 12, we note that a linear relationship exists between ρ_o and Φ^o in the range $20 \leqq \rho_o \leqq 120$ ohm·cm. The linear portion of this curve corresponds to the physiological range of values that might be expected for ρ_o. (Typical values of ρ_o for several biological substances are tabulated in Table II.)

Observation of Fig. 13 reveals an essentially linear relationship between the nerve trunk radius (b) and Φ^o in a log-log plot.

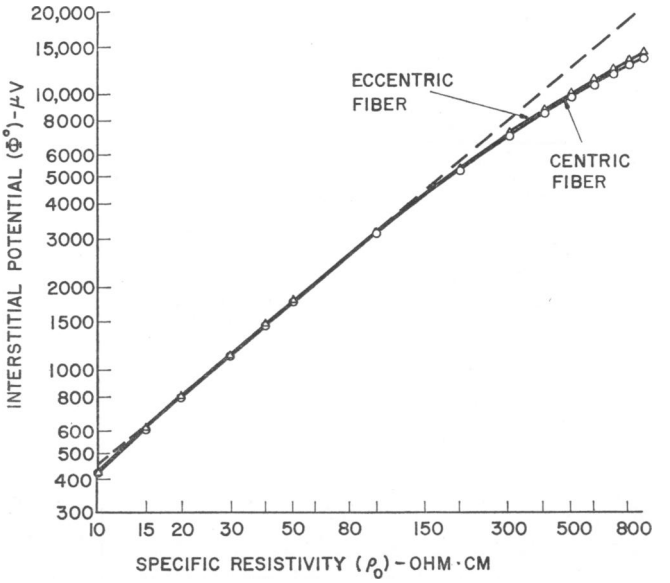

FIGURE 12 Magnitude of interstitial potential vs. specific interstitial resistivity (ρ_o) on a log-log scale, for the eccentric and centrically located active fiber. (z = 0.575 cm)

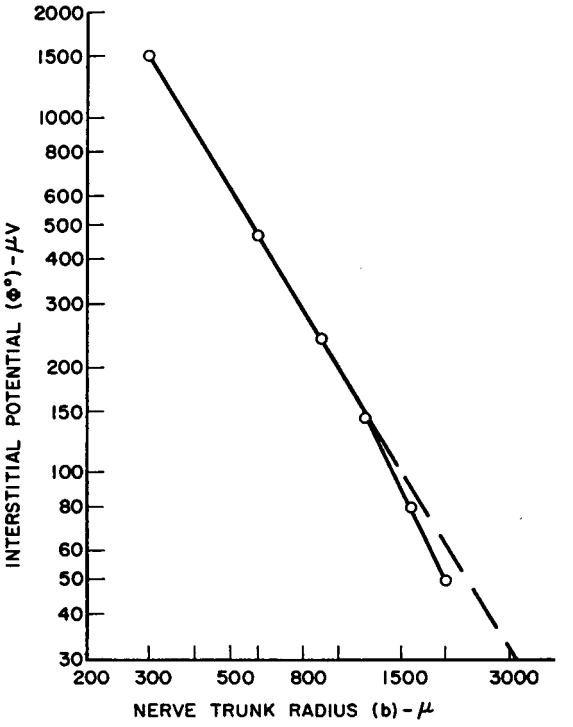

FIGURE 13 Magnitude of interstitial potential vs. nerve trunk radius on a log-log scale. (z = 0.575 cm)

TABLE II

TYPICAL VALUES OF SPECIFIC RESISTIVITY (ρ_o) FOR VARIOUS BIOLOGICAL FLUIDS

Substance	ρ_o *ohm·cm*
Sea water	20.0
Physiological saline	57.0
Ringer's fluid	80.0
Human C.S.F.	64.6
Cat C.S.F.	65.7
Human blood	165.0
Dog blood	153.0

Data taken largely from Geddes and Baker (1967).

The aforementioned results can be understood in at least a qualitative way if it is assumed that interstitial current is essentially axial. This approximation should improve for decreasing cross-sectional area as this tends to confine the current (Offner, 1954). A consequence of this assumption is that the external medium can be represented, electrically, by an effective longitudinal resistance per unit length (r_o) given by

$$r_o = \frac{\rho_o}{A_o} \tag{35}$$

where A_o is the effective cross-sectional area. As a very rough approximation we can express A_o as:

$$A_o = \pi b^2. \tag{36}$$

(This expression neglects the eccentricity of the fiber, the lack of uniformity of axial current and the radial current complication.)

If as a first approximation, we assume the transmembrane potential to be independent of ρ_o and A_o, then the magnitude of the potential field in the interstitial medium depends roughly on the ratio of the external to internal resistance. That is, if we consider these resistances as forming a voltage divider of transmembrane potential (Φ_m), one obtains a measure of the external potential (Φ^o) given by:

$$\Phi^o = \frac{r_o}{r_o + r_i} \Phi_m . \tag{37}$$

Normally $r_o \ll r_i$ so that the factor r_o in the denominator of equation 37 can be neglected,[8] in which case

[8] The computed values of r_o and r_i using equations 35 and 16 respectively, are 0.146×10^5 and 8.325×10^5 ohm/cm. Thus $r_o \ll r_i$.

$$\Phi^o = \frac{r_o}{r_i}\Phi_m = \frac{\rho_o a^2}{\rho_i b^2}\Phi_m . \tag{38}$$

It is interesting to note that for a value of Φ_m of 107 mv,[9] the computed value of Φ^o obtained utilizing equation 38 is 1.82 mv. This value corresponds in order of magnitude to the computed results.

Equation 38 predicts a linear dependence of external potential on ρ_o as observed in Fig. 12, where a unity slope results.[10] When ρ_o becomes sufficiently large so that the assumption $r_o \ll r_i$ is no longer true, then the linear relationship of equation 38 must be replaced by that in 37, which predicts a limiting effect. For example, equation 37 may be rewritten as:

$$\Phi_o = \left[\frac{\rho_o}{\rho_o + \left(\frac{b}{a}\right)^2 \rho_i}\right]\Phi_m . \tag{39}$$

For the values chosen for a and b in this example, the denominator of equation 39 becomes $(\rho_o + 25\rho_i)$. If we consider the term ρ_o in the denominator to be significant only when

$$|\rho_o| \geqq 0.1\,|25\rho_i|, \tag{40}$$

then the calculated value of ρ_o at which there should be a departure from the linear relationship predicted by equation 38 is approximately 234 ohm·cm. This is in agreement with Fig. 13.

Equation 38 also predicts a log-log plot of Φ^o vs. trunk radius (b) to be linear with a slope of -2.[11] In the linear range of Fig. 13, a slope of -1.8 results, which is in reasonable agreement, considering the approximate nature of equation 38.

The rather significant magnitude of interstitial potentials for nerve trunk diameters in the physiological range suggest that under appropriate conditions, interaction or "cross-talk" between fibers within the trunk, could be quite significant. Katz and Schmitt (1940) considered the interaction between two adjacent, isolated crab nerve fibers placed in paraffin oil, under experimental conditions that correspond to those of nerve trunk of small cross-sectional area. They noted significant subthreshold interaction effects and demonstrated that these effects were enhanced by increasing ρ_o. Unfortunately, they did not consider the effect of variation of the artificial interstitial cross-sectional area.

Approximation on Membrane Behavior

In the analysis of the effect of ρ_o and b on the behavior of the active fiber within the nerve trunk it was assumed that the transmembrane potential distribution of the

[9] This is the value of Φ_m at $z = 0.575$ cm, obtained from Fig. 1.

[10] From equation 38: $\log \Phi^o = \log \rho_o + \log w_1$ where $w_1 \equiv \left(\frac{a}{b}\right)^2 \Phi_m/\rho_i$.

[11] From equation 38: $\log \Phi^o = -2 \log b + \log w_2$ where $w_2 \equiv (\rho_o/\rho_i)a^2\Phi_m$.

source fiber and the propagation velocity were unaffected. So long as the effective external resistance is small compared with the axoplasmic resistance,[12] changes in (b^2/ρ_o) should have only a secondary effect on membrane phenomena. That is, under these conditions, the external medium behaves much as a short circuit so that the axoplasm functions effectively as the electrical "load," which is constant. It might be noted that the assumption of the constancy of the membrane sources has been made by Lorente de Nó (1947)[13] in application to an excised model where the external resistance is comparable to (if not in excess of) the internal resistance.

When the effective external resistance is raised to a level where it is no longer negligible, the most significant change in the membrane source properties appears to be in the propagation velocity. This phenomenon has been described by Hodgkin (1939). The specific dependence of propagation velocity (v) on external resistance (r_o) may be explained qualitatively in terms of the electrotonic properties of the active fiber membrane. That is, a significant increase in r_o causes a decrease in the membrane space constant (λ) defined as (Davson, 1964):

$$\lambda = \sqrt{\frac{r_m}{r_o + r_i}} \text{ cm} \tag{41}$$

where r_m is the specific membrane resistance (ohm·cm^2). With a decrease in the space constant, electrotonic current preceding the propagating action potential must flow for a longer period of time in order to excite the same area of membrane (the area immediately adjacent to the active region). This, of course, is reflected in a smaller value of conduction velocity. The dependence of velocity on external resistance affects our results in that the transmembrane potential distribution (Φ_m) is a function of conduction velocity and therefore v appears in each of the derived expressions for potential. Thus the construction of Figs. 12 and 13 may be somewhat in error since they are obtained under the assumption that v is a constant. (Unfortunately, as yet, an analytical expression of the dependence of propagation velocity on r_o has not been developed that would permit making an appropriate correction, or even, of indicating in what range such a correction would be significant.)

So too, the comparison of the external potential waveforms of Fig. 11 must be interpreted qualitatively since the propagation velocities in the two cases are not necessarily the same. Since the external resistance presented to the active fiber is greater in the nerve trunk situation, the fiber will necessarily have a smaller conduction velocity (and consequently, a transmembrane potential distribution of smaller spatial extent) than the fiber situated in the finite medium. If an appropriate correction could be made for v, the resultant surface potential distribution would have a smaller spatial extent than that shown in Fig. 11, thus, more closely resembling the surface distribution of the finite medium fiber.

---

[12] A rough criteria based on equation 38 is that $(\rho_o a^2/\rho_i b^2) \ll 1$.

[13] Specifically, Lorente de Nó assumed that "the internal electromotive forces of the nerve fibers are not altered when the excised nerve is placed in contact with a volume conductor." p. 389.

As for the remaining data presented in this paper, the potential field plots of Figs. 9 and 10 are correct for the specific examples for which they were constructed. Error is introduced however, when one attempts to utilize transmembrane potential distributions under conditions other than that for which they were obtained.

CONCLUSIONS

The behavior of the field of an active cylindrical fiber in both an infinite medium and confined in a nerve trunk has been evaluated quantitatively, based solely on measured transmembrane action potential data. For the infinite medium environment an accurate field plot is readily obtained even though the potentials are in the low microvolt ranges where direct measurement would be quite difficult. The resulting axial variation of the field is triphasic in shape, as would be expected; a monotonic decrease in potential as a function of radius is also computed.

Since the extracellular potential field is very small compared to potentials in the axoplasm, the core conductor model can be utilized satisfactorily provided the external resistance (r_o in Fig. 6) is set equal to zero. This, in effect, restricts further analysis to internal parameters only. The resultant model predicts that the transmembrane current per unit length (i_m) is related to the transmembrane potential Φ_m by the equation

$$i_m = \frac{A_i}{\rho_i} \frac{\partial^2 \Phi_m}{\partial z^2}$$

where A_i is the axoplasmic cross-sectional area and ρ_i its specific resistivity. This relationship, and hence the aforementioned model, is quantitatively verified by the data given in Fig. 5. This work, therefore, constitutes an additional confirmation of the conclusions on the adequacy of the core conductor model stated in an earlier paper (Clark and Plonsey, 1966).

When the fiber lies within a 600 μ diameter nerve trunk (Fig. 7), the quantitative evaluation of interstitial potential reveals that a 20-fold increase in potential can take place, as can be seen from a comparison of Figs. 3 and 10. From Fig. 13, one notes that the cross-sectional area of the trunk has a considerable influence on extracellular potential magnitude. It is also interesting to note, that a trunk radius of 1800 μ corresponds to an essentially infinite medium environment for the fiber.

The specific resistivity of the interstitial medium is also found to have a very pronounced influence on the magnitude of interstitial potential (Fig. 12).

The aforementioned results are of considerable importance in the quantitative investigation of the field interaction existing between adjacent active and inactive nerve fibers in a nerve trunk (as in the case of the medial and lateral giant axons of the ventral nerve cord of lobster or crayfish). The work presented here provides a basis for further study of this important question and indicates that under suitable conditions, interaction or cross-talk between fibers may become significant.

APPENDIX

The following are the derived expressions for the interstitial and external potential in the nerve trunk problem.

$$\Phi^o(\rho, \theta, z) = \frac{2\sqrt{\pi}}{b} \sum_{n=0}^{\infty} \cos n(\theta - \theta_s) \left[\int_0^{\infty} \sum_{n=0}^{3} \left[\left[\frac{K_n\left(\frac{yR_s}{b}\right)}{I_n\left(\frac{yR_s}{b}\right)} + \frac{L_n(y)}{D_n(y)} \right] \cdot I_n\left(\frac{y\rho}{b}\right) \frac{A_i}{B_i} Q_n(y) e^{-y^2/4b^2B_i^2} \cos y\left(\frac{z - C_i}{b}\right) \right] dy \right.$$

$$\left. + \int_0^{\infty} \sum_{i=1}^{3} \left[\frac{\sigma_e}{\bar{\sigma}_{sh}} \frac{\bar{X}_{sh}}{b^2} y \frac{K_n'(y)}{I_n'(y)} \frac{I_n\left(\frac{y\rho}{b}\right)}{D_n(y)} \frac{A_i}{B_i} Q_n(y) e^{-y^2/4b^2B_i^2} \cdot \sin y\left(\frac{z - C_i}{b}\right) \right] dy \right] \quad \text{for} \quad \rho < R_s \tag{A1}$$

$$\Phi^o(\rho, \theta, z) = \frac{2\sqrt{\pi}}{b} \sum_{n=0}^{\infty} \cos n(\theta - \theta_s) \left[\int_0^{\infty} \sum_{i=1}^{3} \left[\left[K_n\left(\frac{y\rho}{b}\right) + \frac{L_n(y)}{D_n(y)} I_n\left(\frac{y\rho}{b}\right) \right] \cdot \frac{A_i}{B_i} Q_n(y) e^{-y^2/4b^2B_i^2} \cos y\left(\frac{z - C_i}{b}\right) \right] dy \right.$$

$$\left. + \int_0^{\infty} \sum_{i=1}^{3} \left[\frac{\sigma_e}{\bar{\sigma}_{sh}} \frac{\bar{X}_{sh}}{b^2} y \frac{K_n'(y)}{I_n'(y)} \frac{I_n\left(\frac{y\rho}{b}\right)}{D_n(y)} \frac{A_i}{B_i} Q_n(y) e^{-y^2/4b^2B_i^2} \cdot \sin y\left(\frac{z - C_i}{b}\right) \right] dy \right] \quad \text{for} \quad \rho > R_s \tag{A2}$$

$$\Phi^e(\rho, \theta, z) = \frac{2\sqrt{\pi}}{b} \sum_{n=0}^{\infty} \cos n(\theta - \theta_s) \left[\int_0^{\infty} \sum_{i=1}^{3} \left[\frac{C_n(y)}{D_n(y)} K_n\left(\frac{y\rho}{b}\right) \frac{A_i}{B_i} Q_n(y) e^{-y^2/4b^2B_i^2} \cdot \cos y\left(\frac{z - C_i}{b}\right) \right] dy \right.$$

$$\left. + \int_0^{\infty} \sum_{i=1}^{3} \left[\frac{\sigma_o}{\bar{\sigma}_{sh}} \frac{\bar{X}_{sh}}{b^2} y \frac{K_n\left(\frac{y\rho}{b}\right)}{D_n(y)} \frac{A_i}{B_i} Q_n(y) e^{-y^2/4b^2B_i^2} \cdot \sin y\left(\frac{z - C_i}{b}\right) \right] dy \right] \quad \text{for} \quad \rho < R_s \tag{A3}$$

where

$$I_n'(y) = y/b\left[\frac{n}{y} I_n(y) + I_{n+1}(y)\right] \tag{A4}$$

$$K_n'(y) = y/b\left[\frac{n}{y} K_n(y) - K_{n+1}(y)\right] \tag{A5}$$

$$Q_n(y) \equiv \frac{-(2 - \delta_n{}^0) I_1\left(\frac{ya}{b}\right) I_n\left(\frac{yR_s}{b}\right)}{2\pi\left[\frac{\sigma_o}{\sigma_i} K_1\left(\frac{ya}{b}\right) I_0\left(\frac{ya}{b}\right) + I_1\left(\frac{ya}{b}\right) K_0\left(\frac{ya}{b}\right)\right]} \tag{A6}$$

$$E_n(y) \equiv [\sigma_e I_n(y) K_n'(y) - \sigma_o I_n'(y) K_n(y)] \tag{A7}$$

$$C_n(y) \equiv -\frac{\sigma_o}{b}\left[1 + \frac{\bar{\sigma}_{sh}^2 + (y/b)^2 \bar{X}_{sh}^2}{\sigma_o \sigma_e \bar{\sigma}_{sh}} \frac{E_n(y)}{I_n'(y) K_n'(y)}\right] \tag{A8}$$

$$D_n(y) \equiv \left[\frac{\sigma_o \sigma_e}{\bar{\sigma}_{sh}} I_n'(y) K_n'(y) + 2E_n(y) + \frac{\bar{\sigma}_{sh}^2 + (y/b)\bar{X}_{sh}^2}{\sigma_o \sigma_e \bar{\sigma}_{sh}} \frac{E_n(y)}{I_n'(y) K_n'(y)}\right] \tag{A9}$$

$$L_n(y) = -K_n'(y)\left[\frac{\sigma_o \sigma_e}{\bar{\sigma}_{sh}} K_n'(y) + (\sigma_e - \sigma_o) K_n(y) + \left(K_n'(y) + \frac{\bar{\sigma}_{sh}^2 + (y/b)^2 \bar{X}_{sh}^2}{\sigma_o \sigma_e \bar{\sigma}_{sh}} (\sigma_o - \sigma_e) K_n(y)\right) \frac{E_n(y)}{I_n'(y) K_n'(y)}\right] \tag{A10}$$

The derived expression for trans-sheath potential is:

$$\Phi_{sh}(\theta, z) = \frac{2\sqrt{\pi}}{b} \sum_{n=0}^{\infty} \cos n(\theta - \theta_s) \cdot \left[\int_0^{\infty} \sum_{i=1}^{3} \left[[(D_n(y) - C_n(y)) K_n(y) + L_n(y) I_n(y)] \cdot \frac{A_i}{B_i} \frac{Q_n(y)}{D_n(y)} e^{-y^2/4b^2 B_i^2} \cos y\left(\frac{z - C_i}{b}\right)\right] dy + \int_0^{\infty} \sum_{i=1}^{3} \left[\frac{\bar{X}_{sh}}{\bar{\sigma}_{sh} b^2}\left(\frac{\sigma_e K_n'(y)}{I_n'(y)} I_n(y) - \sigma_o K_n(y)\right) \cdot \frac{A_i}{B_i} \frac{Q_n(y)}{D_n(y)} e^{-y^2/4b^2 B_i^2} \sin y\left(\frac{z - C_i}{b}\right)\right] dy\right] \tag{A11}$$

This work was supported in full by Public Health Service Grants HE 10417 and HM 1090 from the National Institutes of Health.

Received for publication 11 January 1968 and in revised form 4 April 1968.

REFERENCES

BRAZIER, M. A. B. 1960. The Electrical Activity of the Nervous System. Pitman Publishing Co., London, England. 2nd edition.

CASELLA, C., and B. TACCARDI. 1965. *In* International Symposium on the Electrophysiology of the Heart. B. Taccadi and G. Marchetti, editors. Pergamon Press, Inc., New York. 153.
CLARK, J. W., and R. PLONSEY. 1966. *Biophys. J.* **6**:95.
DAVSON, H. 1964. Textbook of General Physiology. Little, Brown and Co., Boston, Mass. 697.
GEDDES, L. A., and L. E. BAKER. 1967. *Med. Biol. Eng.* **5**:271.
GESELOWITZ, D. 1966. *Biophys. J.* **6**:691.
GRANIT, R., L. LEKSELL, and C. R. SKOGLUND. 1944. *Brain.* **67**:125.
GRAY, A., and G. B. MATTHEWS. 1966. A Treatise on Bessel Functions and their Application to Physics. Dover Publications, Inc., New York.
LORENTE DE NÓ, R. 1947. *Studies Rockefeller Inst. Med. Res.* **132**:389.
OFFNER, F. 1954. *Electroencephalog. Clin. Neurophysiol.* **6**:507.
PATLAK, C. S. 1955. *Bull. Math. Biophys.* **17**:287.
TASAKI, I. 1953. Nervous Transmission. C. C. Thomas Publisher, Springfield, Ill.
TASAKI, I. 1959. *In* Handbook of Physiology. Section I: Neurophysiology. American Physiological Society, Washington, D.C. 74.
TASAKI, I. 1964. *J. Neurophysiol.* **27**:1200.
WATANABE, A., and H. GRUNDFEST. 1961. *J. Gen. Physiol.* **45**:267.
WEBER, H. 1873. *Borchardt's J. Math.* **76**:1.